Dual mode fiber optic SPR chemical microsensor

Lin C.-W.*[a], Liou Y.-T.[a], Huang C.-Y.[b], Chiu J.-P.[b], Kou T.-S.[a,b]
[a] Institute of Biomedical Engineering, National Taiwan University, Taipei, Taiwan
[b] Department of Electrical Engineering, National Taiwan University, Taipei, Taiwan

ABSTRACT

A fiber optic microsensor is described which utilizes the surface plasmon resonance (SPR) effect to detect the chemical environment surrounding the fiber. The sensor is a multimode step index optic fiber, which is constructed by removing the fiber cladding layer with hot sulfuric acid and coated with gold film on fiber core and on distal end. The changes in the light reflectivity are recorded as SPR spectra, which are highly sensitive to the optical properties of the samples adjacent to the sensor surface. The incident light is guided through a splitter to excite and record SPR in both visible and near infrared (NIR) regions. The NIR spectrum has a larger and sharper resonant peak than visible one. It thus provides a more sensitive mechanism to probe the vicinity of interface for biochip applications.
Keywords: Surface Plasmon Resonance, sensor, fiber, visible, near infrared

1. INTRODUCTION

The surface plasmon resonance (SPR) has been widely applied to biosensing since 1980s [1, 2]. Usually, one can apply light or electrons on the interface of metal and dielectric to generate SPR signal [3, 4]. It provides a highly sensitive method to probes the optical properties of sample of interest. Either with single wavelength multiple angle (SWMA) or multiple wavelength single angle (MWSA), the SPR occurs when the wave vectors of incident light matches the wave vectors of the surface plasmons. The changes in the reflective intensity (reflectance) are recorded as SPR spectra [5, 6]. The SPR spectrum is highly sensitive to the optical properties of the dielectric (biomolecules) adjacent to the metal surface. Thus, SPR is suitable for exploring the biophysical and biochemical interactions of protein-membrane and protein-protein in the biochips [7-10]. Recently, this optical phenomenon has been extended to explore the region of near infrared (NIR) excitation [11]. In this paper, we will first present an analytical system to deal with the signal from Kretshmann configuration of SPR experimental setup in both visible and NIR wavelength region. According to the theoretical calculation, the NIR spectrum has a larger and sharper resonant peak than visible one. A two-channel spectrograph system is then used to verify the calculation results.

2. METHODOLOGY

2.1. Theoretical background

More details of the theoretical derivation can be found in the excellent book of surface plasmon [3]. Briefly, a p-polarized light incident on a x_z plane in Kretshmann configuration, as depicted in the figure 1.
For dielectric layer, Z<0:

$$\vec{H}_2 = [0, H_{y2}, 0]e^{j(k_{x2}x + k_{z2}z - \omega t)} \quad (1)$$

$$\vec{E}_2 = [E_{x2}, 0, E_{z2}]e^{j(k_{x2}x + k_{z2}z - \omega t)} \quad (2)$$

For metal layer, z>0:

$$\vec{H}_1 = [0, H_{y1}, 0]e^{j(k_{x1}x - k_{z1}z - \omega t)} \quad (3)$$

$$\vec{E}_1 = [E_{x1}, 0, E_{z1}]e^{j(k_{z1}x - k_{z1}z - \omega t)} \quad (4)$$

where, $\overrightarrow{E_1}$: Electric field in metal (1); $\overrightarrow{H_2}$:Magnetic field in dielectric (2); k_{zi} : Z component of the wave vector in medium I; ω : Angular frequency of the incident light; C: Speed of light; ε_i :Dielectric function of medium i; ε_i ': Real part of ε_i ; ε_i ": Imaginary part of ε_i .
These fields should fulfill Maxwell's equations and continuous boundary conditions. And the subsequent derivation would lead to the field penetration of both electrical and magnetic components in the metal and dielectric layer. It thus allows the calculation of the penetration depth of the evanescent field on the interface.

Biophotonics Instrumentation and Analysis, Arthur E. T. Chiou, Halina Podbielska, Steven L. Jacques,
Editors, Proceedings of SPIE Vol. 4597 (2001) © 2001 SPIE · 0277-786X/01/$15.00

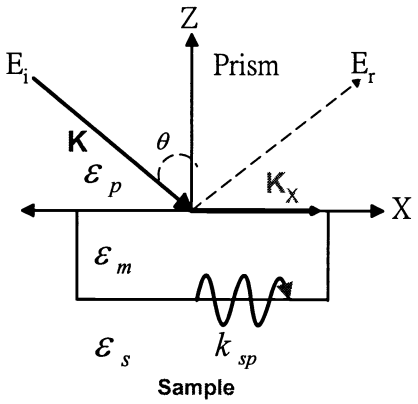

Fig. 1: Illustration of SPR excitation by Kretshmann configuration. A p-polarized light is incident on x_z plane through a prism and the surface plasmon wave generated on the interface of metal and dielectric (sample).

The optical excitation of plasmons is possible only when a proper coupling of light to metal. This can be accomplished by using the attenuated total reflection (ATR) method with a prism coupler. Under the matching condition of parallel component of incident wave vector to the surface plasmons resonance wave vector, one can calculate the reflective spectrum with known thickness and refractive index. However, the p-polarized multilayer reflectance of the electric field can be calculated more efficiently by the matrix method. A three-layer configuration of BK7/Au/H_2O is used to calculate the SPR spectra in visible region by using both angle and wavelength modulation. The extension to the NIR region is calculated to show the difference in resonant spectra. A six-layer biosensor model (coupler/metal/linker/ligand/analyte/buffer) is constructed to simulate the possible applications in the near future.

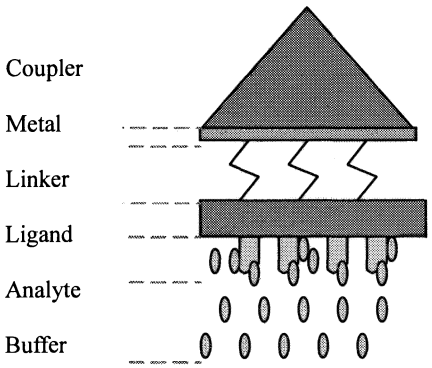

Fig. 2: A six layer biosensor model for SPR simulation.

For extracting the optical parameters (*n*, *k*, and *d*) from measured SPR spectrum, a nonlinear regression method is implemented in the system as shown in the follows.
Fitting the minimum value, with assumed m sets of SPR spectral data,

$$Min \left(\sum_{i=1}^{m} [y_i - f(\vec{x}_i, \vec{\theta})]^2 \right) \tag{5}$$

where, $\vec{x}_i$: the i_{th} point of spectrum [width, depth, site]; y_i : the i_{th} point of reflectance; y= $f(\vec{x}, \vec{\theta})$: the regression spectrum to be fitted; $\vec{\theta}$ is a function of [n, k, d].

2.2 Fiber Sensor and System Setup

A fixed length of multimode step index silica/silicon optical fiber is used constructed the SPR fiber sensor. After polished both ends and removed the cladding with sharp knife, the exposed section of the core fiber is treated with standard cleaning procedures of hot distilled water, acetone, ethanol and isopropanol. It is then put into a thermal evaporator to deposit 50 nm Au as the metal layer for SPR sensing with static hanging position. The same procedure can

result in an average roughness of 3 nm on a planar glass wafer. The distal end of the fiber is then packed with standard SMA connector for the connection to the rest of the measurement system. The spectrographic measurement system is shown as in the figure 3. Other than the fabricated fiber sensor, a halogen lamp as light source brings the light through a tri-furcated optical fiber bundle. The reflective light is collected and detected by a two-channel miniature spectrograph system (SD-2000, Ocean Optics Inc., California). The spectral signals are digitized by using a PCMCIA data acquisition card (DaqCard^{TM}-700, National Instruments, Austin). The control software was programmed on a portable computer (Acer 370PCX, Taiwan) by using LabVIEW 5.01 (National Instruments, Austin).

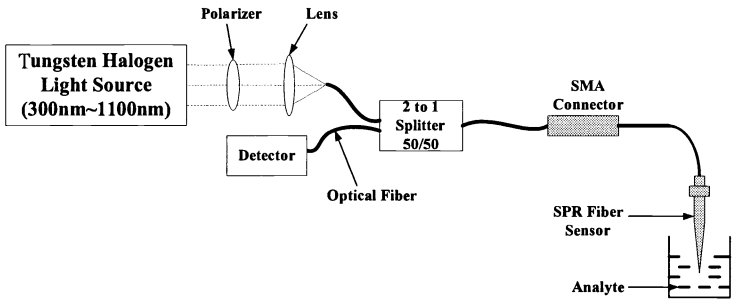

Fig. 3: Block diagram of SPR fiber measurement system.

3. RESULTS

3.1 Theoretical Calculation

The penetration depth of the evanescent wave on 50 nm thickness of Au film and air is shown as in the figure 4. With 539.1 nm incident light, the characteristic length of such a field penetration in the Au and air are 30.9 nm and 204.3 nm, respectively.

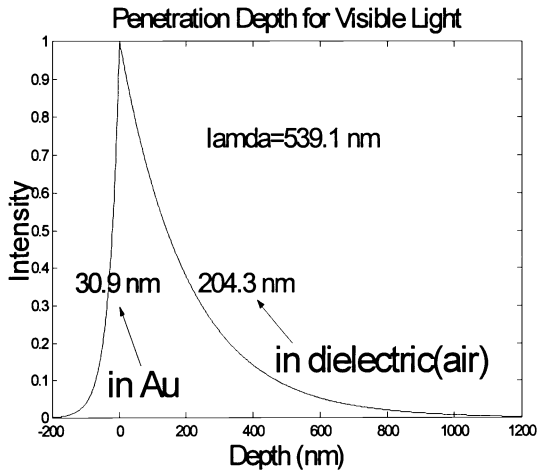

Fig. 4: Exponential decay of the evanescent field. The penetration depth is 30.9nm and 204.3nm in Au and in dielectric, respectively.

Both angular and wavelength interrogation of the SPR can also be simulated by 3-layer (BK7/Au/H_2O) configuration and the results are shown as in the figure 5. In the angular modulation (fig.5a), two different wavelengths (600 nm and 750 nm) have two distinguished resonance peaks around 67 and 76 degree, respectively. Note that near infrared one has narrower half band width and higher peak amplitude than the visible light. In the wavelength modulation (fig. 5b), two different incident angles (72 and 68.5 degree) have different resonance peaks around 640 nm and 710 nm, respectively. In 6-layer biosensor model, the advantages of NIR excitation become more significant due to the effective penetration depth limited by the linker layer, which is 50 nm in this case. In the figure 6a, with 633 nm incident light, the reflective resonant spectrum not only has broader peak width but also shifts toward 85 degree, which is difficult for most of the instrument setup. However, with 1152 nm incident light, the same configuration has significant changes in the peak amplitude, width, and position, which result in better angle resolution and thus the signal to noise ratio.

The backward calculation for the prediction of undetermined sample has to do by nonlinear curve fitting process. As a

demonstrative example, one simulated resonant spectrum is first generated then curve fitting by above mentioned techniques to optimally decide the critical parameters (n, k, t). One of the solutions of the simulated bio-analyte is shown in figure 7. Note that there are multiple valid solutions from such a regression analysis. It thus requires a calibration method to verify the results in the future.

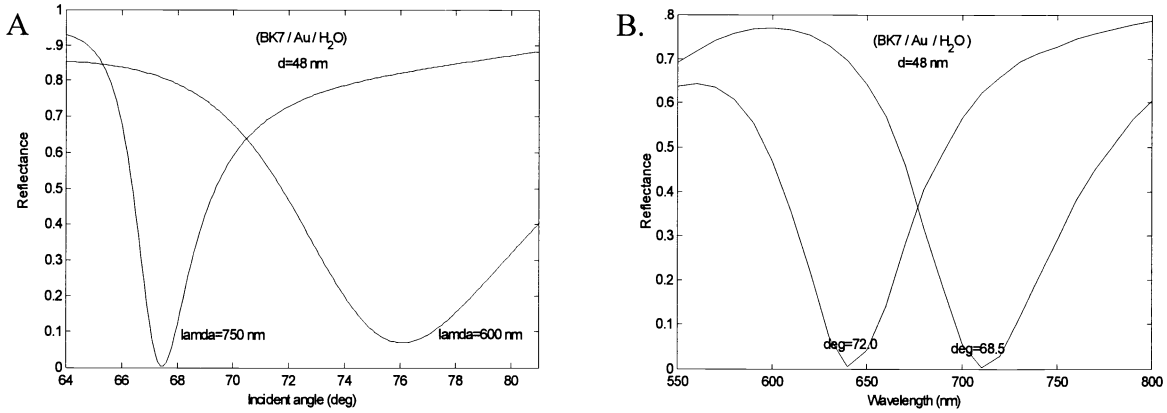

Fig. 5: The calculation results of 3-layer (BK7/Au (50 nm)/H_2O) model SPR spectra with (a) angular interrogation with two different wavelength, 600 nm and 750 nm, respectively, (b) wavelength interrogation with two different incident angle, 72 and 68.5, respectively. Note that in the fist graph, 750 nm results in a sharper resonant spectrum.

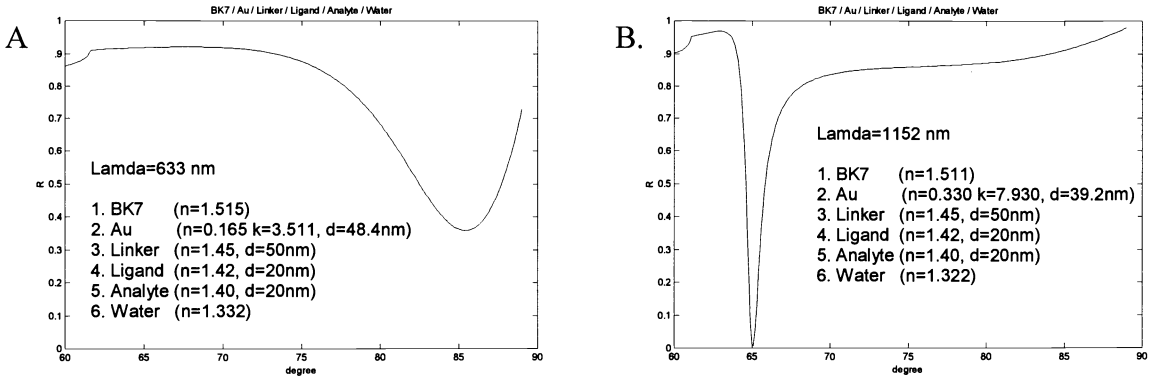

Fig. 6: The calculation results of 6-layer biosensor model (BK7/Au/Linker (50 nm)/Ligand/Analyte/Buffer) SPR spectra with (a) 633 nm and (b) 1152 nm. The latter has significant improvements in resonant peak amplitude, width, and angle position.

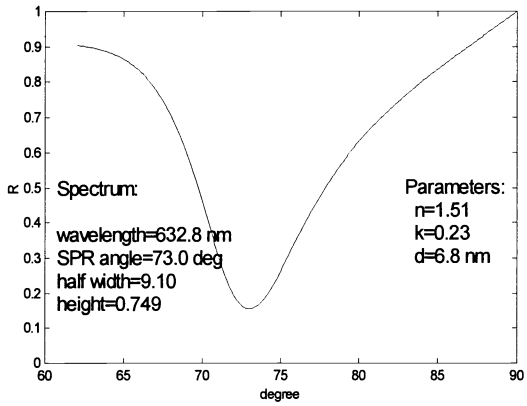

Fig. 7: Optical parameters calculated from SPR spectrum by nonlinear regression method and supplementary calibration buffer.

3.2 Fabricated fiber SPR sensor

The fabricated fiber sensor according to above mentioned procedures can be seen in the figure 8. Under polarized light, the translucent green-yellowish color of the fiber indicts the successful deposition of thin film of gold as the base of further modification (fig. 8a). The packed fiber sensor with a protective sleeve and SMA connector is then integrated with all the necessary instruments as shown in the figure 8b and 8c. The measured spectra from this system in distilled water and pure ethanol has two distinguished resonance peaks after subtracted from the background. The resonance peak shifts from 641 nm in water to 643 nm in ethanol. While in the NIR channel, it shifts from 710 nm to 712 nm.

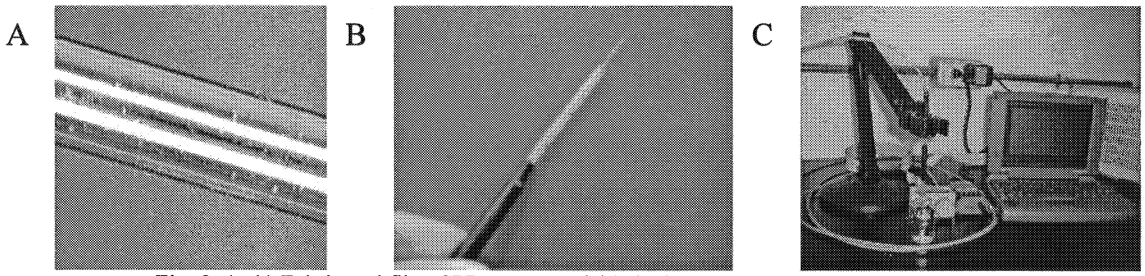

Fig. 8: (a, b) Fabricated fiber SPR sensor and (c) the integrated measurement system.

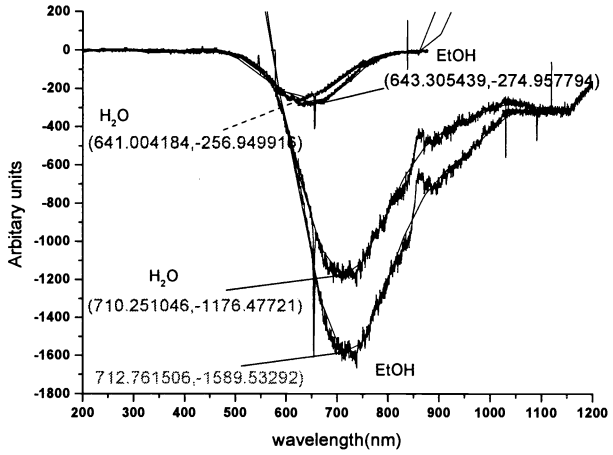

Fig. 9: Resonance spectra of fabricated dual mode fiber SPR sensor in distilled water (n=1.33) and ethanol (n=1.365). The resonance peaks are 641 nm and 643 nm in the visible region, 710 nm and 712 nm in the NIR region, respectively.

4. DISCUSSION

SPR is a sensitive tool for exploring the biophysical and biochemical interactions in the vicinity of interface. It has been extensive used in the thin film investigation since 1950s. Recently, it extends to biomedical applications include gene detection, protein-membrane and protein-protein interactions. It is a label-free method, which has apparent advantage over other techniques. In this paper, we use a previous reported SPR simulation program deal with the signal from Kretshmann configuration of SPR experimental setup in both visible and NIR regions [11]. It is capable of analyzing the spectral signal from wavelength and angle interrogation SPR spectra. With the collective database of optical parameters of various materials used as thin films, which include metals, semiconductors, insulators, and compounds in this system, it would allow for the calculations of both forward and backward models. To calculate the possible optimal solutions, a ringer solution is suggested as calibration standard to normalize the spectra for optical parameters best fitted by nonlinear multiple regression. The major consideration is to help to narrow down the search range of parameters and try to get the optimal solution closer to the real condition. We adopted mixed gradient descent and simplex downhill search for optimal solution. However, there might be multiple solutions by the regression analysis. However, due to the existences of infinite solutions, we would need a calibration procedure to verify the answer for unknown samples. This procedure can be intuitive or explicit by means of multiple metals or thickness with known optical parameters.

The micro fabrication procedures for fiber SPR sensor would need further improvements to enhance the performance. Right now, it is very difficult to handle the circular deposition on to fiber surface. Wet chemical deposition with Au nano particles has been tried and seems a rather promising procedure for further investigations.

5. CONCLUSIONS

The accomplished goals include simulating SPR phenomena, constructing multilayers, predicting spectra, recording experimental data, and analyzing experimental spectrum in the analytical system. This study devises an analytical system which can real-time analyze the wavelength and angular interrogation of Kretshmann SPR configuration. On account of plenty organic and inorganic material database, the analytical system supports a wide range of SPR multilayer spectrum analysis. With regression analysis, optical parameters of the unknown sample can be calculated from measured spectra. According to the theoretical calculation, the NIR spectrum has a larger and sharper resonant peak than visible one. A two-channel spectrograph system is then used to verify the calculation results.

ACKNOWLEDGEMENTS

This work is supported by National Science Council, Taiwan, R.O.C., NSC90-2323-B002-005.

REFERENCES

1. B. Liedberg, C. Nylander, and I. Lundstrom, "Surface plasmons resonance for gas detection and biosensing," *Sensors and Actuators*, **4**, pp. 299-304, 1983.
2. J.G. Gordon II, and S. Ernst, "Surface plasmons as a probe of the electrochemical interface," *Surface Sci.*, **101**, pp. 499-506, 1980.
3. H. Raether, *Surface Palsmons on smooth and rough surfaces and on gratings*, ***ch.2***, Springer-Verlag, Berlin, 1988
4. K. Kurosawa, R.M. Pierce, S. Ushioda, and J.C. Hemminger, "Raman scattering and attenuated-total-reflection studies of surface-plasmon polarizations" Phys. Rev. B, **33**, pp. 789-798, 1986
5. J. Homola, S. S.Yee, and G. Gauglitz, "Surface plasmon resonance sensor : review, " *Sensors and Actuators B*, **54**, pp. 3-15, 1994.
6. Z. Salamon, H.A. Macleod, and G. Tollin, " Surface plasmon resonance spectroscopy as a tool for investigating the biochemical and biophysical properties of membrane protein system. I: Theoretical principles," *Biochimica et Biophysica Acta*, **1331**, pp. 117-129, 1997.
7. Z. Salamon, H.A. Macleod, and G. Tollin, " Surface plasmon resonance spectroscopy as a tool for investigating the biochemical and biophysical properties of membrane protein system. II: Applications to biological systems," *Biochimica et Biophysica Acta*, **1331**, pp. 131-152, 1997.
8. V. Silin and A. Plant, "Biotechnological applications of surface plasmon resonance", *TIBTECH*, **15**, pp. 353-359, 1997.
9. E. Saenko, A. Sarafanov, N. Greco, M. Shima, K. Loster, H. Schwinn, and D. Josic, "Use of surface plasmon resonance for studies of protein-protein and protein-phospholipid membrane interactions", *J. of Chromatography A*, **852**, pp. 59-71, 1999.
10.. J. Haimovich, D. Czerwinski, C. P. Wong, and R. Levy, "Determination of anti-idiotype antibodies by surface plasmon resonance," *J. of Immunological Methods*, **214**, pp. 113-119, 1998.
11. C.-Y. Huang, C.-W. Lin, and T.-S. Kou, "An analytical system for multilayer surface plasmon resonance signal", IEEE/EMBS 23rd Annual International Conference, Istanbul, Turkey, 2001

*cwlin@cbme.mc.ntu.edu.tw; phone 886-2-23912217; fax 886-2-3940049; http://ibme.mc.ntu.edu.tw; BioMEMS Laboratory, Institute of Biomedical Engineering, College of Engineering and College of Medicine, National Taiwan University,; No.1, Sec. 1, Jen-Ai Road, Taipei, Taiwan, 100, R.O.C.